

Enhancement effect of cumulative second-harmonic generation by closed propagation feature of circumferential guided waves*

Guang-Jian Gao(高广健)¹, Ming-Xi Deng(邓明晰)^{2,†}, Ning Hu(胡宁)², and Yan-Xun Xiang(项延训)^{3,‡}

¹Department of Physics, Army Logistics University, Chongqing 401331, China

²College of Aerospace Engineering, Chongqing University, Chongqing 400044, China

³School of Mechanical and Power Engineering, East China University of Science and Technology, Shanghai 200237, China

(Received 8 November 2019; revised manuscript received 11 December 2019; accepted manuscript online 17 December 2019)

On the basis of second-order perturbation approximate and modal expansion approach, we investigate the enhancement effect of cumulative second-harmonic generation (SHG) of circumferential guided waves (CGWs) in a circular tube, which is inherently induced by the closed propagation feature of CGWs. An appropriate mode pair of primary- and double-frequency CGWs satisfying the phase velocity matching and nonzero energy flux is selected to ensure that the second harmonic generated by primary CGW propagation can accumulate along the circumference. Using a coherent superposition of multi-waves, a model of unidirectional CGW propagation is established for analyzing the enhancement effect of cumulative SHG of primary CGW mode selected. The theoretical analyses and numerical simulations performed directly demonstrate that the second harmonic generated does have a cumulative effect along the circumferential direction and the closed propagation feature of CGWs does enhance the magnitude of cumulative second harmonic generated. Potential applications of the enhancement effect of cumulative SHG of CGWs are considered and discussed. The theoretical analysis and numerical simulation perspective presented here yield an insight previously unavailable into the physical mechanism of the enhancement effect of cumulative SHG by closed propagation feature of CGWs in a circular tube.

Keywords: circumferential guided wave, second-harmonic generation (SHG), enhancement effect of cumulative SHG, closed propagation feature

PACS: 43.35.+d, 43.25.+y, 43.20.Mv

DOI: 10.1088/1674-1056/ab628d

1. Introduction

Circular tubes widely serve in chemical, pharmaceutical, food and power engineering industries due to their excellent mechanical properties.^[1,2] As an effective means, ultrasonic guided waves have been effectively used for nondestructive assessment of circular tubes.^[3-6] It is known that the guided wave modes propagating in circular tubes can be classified into two types: axial mode propagating along the axial direction (including longitudinal,^[7] torsional,^[8] and flexural mode^[9]) and circumferential mode propagating along the circumferential direction.^[10,11] The circumferential mode of guide wave propagation in a circular tube is referred to as circumferential guided wave (CGW), where its propagation path is closed and the corresponding standing wave is formed in the radial direction.

Due to the closed propagation feature of CGW mode (namely, its propagation path is closed), it is especially suitable for detecting the radial and axial cracks in the circular tube with a larger diameter.^[10,11] Qu *et al.* laid a groundwork for investigations of dispersion relations of CGWs in a hollow cylinder.^[12] Then some analytical and experimental investigations of propagation feature of CGWs have been performed.^[13-16] Compared with the axial guided wave

modes, the CGWs have some unique advantages in nondestructive assessment of circular tube structures. Firstly, when the axial length of a circular tube is relatively short, the axial guided waves can readily be affected by the end-face reflections, while the CGWs can completely avoid the influence of the end-face reflections because they propagate only along the circumference of the given circular tube. Secondly, due to the closed propagation feature of CGWs, the finite-duration CGW signal can propagate periodically along the circumference of the circular tube (or it can be repeatedly detected at the same position of the circular tube), which may make CGWs show more abundant nonlinear wave phenomena compared with the axial guided waves, Lamb waves and SH plate waves investigated previously.^[17-20]

Considering the fact that the nonlinear ultrasonic technique is much more sensitive to early damage in materials than that based on the linear feature of ultrasonic wave propagation,^[21-25] and that the CGWs have the unique advantages in nondestructive assessment of circular tube structures, it is expected that nonlinear CGWs can be used to effectively assess the early damage in circular tubes. Recently, Gao *et al.* established a theoretical model to analyze the effect of second-harmonic generation (SHG) of primary CGW propagation.^[26]

*Project supported by the National Natural Science Foundation of China (Grant Nos. 11834008, 11704410, 11632004, 11474361, and U1930202).

†Corresponding author. E-mail: dengmx65@yahoo.com

‡Corresponding author. E-mail: yxxiang@ecust.edu.cn

Then, Deng *et al.* experimentally demonstrated that the second harmonic generated by propagation of primary CGW mode satisfying the phase velocity matching and nonzero power flux could grow along the circumference of the tube.^[27] On this basis, it has been experimentally validated that the level of the accumulated damage in a circular tube can effectively be revealed by the acoustic nonlinearity parameter of primary CGW propagation through one full circumference.^[28] Furthermore, Li *et al.* analyzed the nonlinear feature of CGW propagation in a composite circular tube.^[29–32] Although it is known that the nonlinear CGWs have the potential for non-destructive assessment of circular tube structures, the physical mechanism how the closed propagation feature of CGWs influences the effect of SHG of primary CGW still remains unrevealed. Specifically, it is necessary to investigate the enhancement effect of cumulative SHG, which is inherently induced by the closed propagation feature of CGWs.

In this paper, modeling and simulation of the enhancement effect of cumulative SHG by the closed propagation feature of CGWs will be conducted. The corresponding theoretical predictions will be examined by the finite element (FE) simulation. Moreover, the potential for applications of the enhancement effect of cumulative SHG of CGWs will be considered and discussed. The results obtained yield a previously unavailable insight into the physical mechanism of the enhancement effect of cumulative SHG by closed propagation feature of CGWs in the given circular tube.

2. Theoretical fundamentals

2.1. SHG of CGW propagation

The schematic diagram of a circular tube with inner radius R_1 and outer one R_2 is shown in Fig. 1, where the tube material is assumed to be isotropic, homogeneous and dispersionless. It should be noted that the model shown in Fig. 1 is also used for the FE simulations, where the excitation sources, as well as other settings will be described in more detail later in Section 3.

According to the stress-free boundary conditions on the inner and outer surfaces of the circular tube, both the dispersion relations for CGW propagation and the corresponding displacement fields can readily be determined.^[26] When the primary CGW with the driving frequency f and order index l propagates clockwise along the circumference of the circular tube shown in Fig. 1, the corresponding mechanical displacement field can formally be given by

$$U^{(f,l)} = U^{(f,l)}(r) \exp[jN^{(f,l)}\theta - j\omega t], \quad (1)$$

where $\omega = 2\pi f$ is the angular frequency, $N^{(f,l)} = \omega R_2 / c_p^{(f,l)}$ and $c_p^{(f,l)}$ are the dimensionless angular wave number and the phase velocity of the l^{th} primary CGW mode, $U^{(f,l)}(r)$ is the

corresponding displacement field function of the l^{th} primary CGW mode.

Due to the geometric nonlinearity and the inherent elastic nonlinearity of solid, within a second-order perturbation, accompanying propagation of the l^{th} primary CGW along the tube circumference, there are the traction stress tensors of double the fundamental frequency, denoted by $P^{(\text{NL})}$, on the inner and outer surfaces of the circular tube. In addition to $P^{(\text{NL})}$, there is the bulk driving force at the double fundamental frequency, denoted by $F^{(\text{NL})}$, inside the circular tube. The formal expressions of $P^{(\text{NL})}$ and $F^{(\text{NL})}$ are presented in Refs. [26,28].

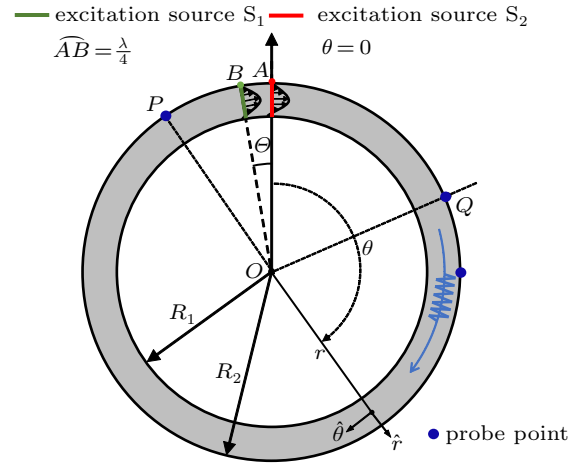


Fig. 1. Schematic diagram of the circular tube used for analyzing CGW propagation, where \hat{r} and $\hat{\theta}$ are the unit vectors along the radial and circumferential directions.

Based on the modal expansion approach for waveguide excitation,^[26,33] both of $P^{(\text{NL})}$ and $F^{(\text{NL})}$ generate a series of double-frequency CGW (DFCGW) modes. In other words, the linear sum of a series of DFCGW modes generated by $P^{(\text{NL})}$ and $F^{(\text{NL})}$ constitutes the second-harmonic field (denoted by $U^{(2f)}$) of the l^{th} primary CGW mode, namely,^[26,28,33]

$$U^{(2f)} = \sum_m A_m(\theta) U^{(2f,m)}(r), \quad (2)$$

where $A_m(\theta)$ and $U^{(2f,m)}(r)$ are, respectively, the expansion coefficient and the field function of the m^{th} DFCGW mode generated. Based on the previous derivation,^[26] the formal expression of $A_m(\theta)$ is given by

$$A_m(\theta) = \frac{(f_m^{\text{surf}} + f_m^{\text{vol}})}{4P_{mm}} \left[\frac{\sin(\Delta N \theta)}{\Delta N} \exp(j\Delta N \theta) \right] \exp[jN^{(2f,m)}\theta], \quad (3)$$

where $\Delta N = [N^{(f,l)} - N^{(2f,m)}]$ is used to describe the dispersion degree between the l^{th} primary CGW mode and the m^{th} DFCGW mode, $N^{(2f,m)} = 2\omega R_2 / c_p^{(2f,m)}$ and $c_p^{(2f,m)}$ are the dimensionless angular wave number and the phase velocity of the m^{th} DFCGW mode; P_{mm} is the average power flow of m^{th} DFCGW mode (per unit width, perpendicular to the tube section); f_m^{vol} and f_m^{surf} are the bulk and surface driving source, which are associated with the second-order traction stress tensor $P^{(\text{NL})}$ and the second-order bulk driving

force $\mathbf{F}^{(NL)}$, respectively. The formal expressions of $U^{(f,l)}(r)$ and $U^{(2f,m)}(r)$, as well as P_{mm} , f_m^{vol} and f_m^{surf} are also derived in Ref. [26]. When both the nonzero energy flux (i.e., $(f_m^{\text{vol}} + f_m^{\text{surf}})/4P_{mm} \neq 0$) and the phase velocity matching (i.e., $\Delta N = 0$ or $\Delta N \approx 0$) are simultaneously satisfied, the second harmonic field [i.e., $U^{(2f)}$ in Eq. (2)] generated by propagation of the l^{th} primary CGW is mainly dependent on the m^{th} DFCGW, and the contribution of other DFCGW modes to the second-harmonic field can be negligible.[26] Under this circumstance, Equation (2) can thus be rewritten as

$$U^{(2f)} = \frac{(f_m^{\text{vol}} + f_m^{\text{surf}})}{4P_{mm}} \cdot \theta \cdot U^{(2f,m)}(r) \cdot \exp[jN^{(2f,m)}\theta]. \quad (4)$$

Obviously, the magnitude of second-harmonic field will grow linearly with the circumferential angle θ . Until now, the solution of cumulative second harmonic of primary CGW propagation in a circular tube has been exactly determined using a second-order perturbation and modal expansion analysis approach.

2.2. Enhancement effect of cumulative second harmonic

Within a second-order perturbation, the amplitude of primary CGW signal can be regarded to be unchanged when the acoustic attenuation of solid is neglected, while the amplitude of cumulative second harmonic generated will grow linearly with the circumferential angle θ (see Eq. (4)). Specifically, at the same position of the circular tube in Fig. 1 (e.g., at the circumferential angle θ or $\theta + 2n\pi$; n is an integer), for the desired mode pair [i.e., the l^{th} CGW (primary) and the m^{th} DFCGW (generated)], the amplitude of the l^{th} CGW signal (denoted by A_1) received at θ for the first time is the same

as that received at $\theta + 2n\pi$, i.e., the amplitude of the primary CGW signal (A_1) will be kept unchanged even if the CGW signal propagates n cycles around the circumference. In contrast, the amplitude of cumulative second-harmonic signal (denoted by A_2) received at $\theta + 2n\pi$ will be $(\theta + 2n\pi)/\theta$ times that received at θ . Clearly, this effect (i.e., the enhancement effect of cumulative SHG) is induced by the closed propagation feature of CGWs. It is noticeable that the effect of cumulative second harmonic of primary CGW mode is completely different from that induced by propagation of primary guided wave whose propagation path is not closed (e.g., Lamb wave, SH plate wave, or axial guided wave in circular tube). Combining Eqs. (1) and (4), the relative nonlinear acoustic parameter, defined by $\beta_R = A_2/A_1^2$, [21] can be formally expressed as

$$\beta_R = \left| \frac{f_m^{\text{vol}} + f_m^{\text{surf}}}{4P_{mm}} \right| \cdot \left| \frac{U^{(2f,m)}(r)}{[U^{(f,l)}(r)]^2} \right|_{r=R_2} \theta. \quad (5)$$

Clearly, at the same position of the circular tube, the relative nonlinear acoustic parameter β_R measured at $\theta + 2n\pi$ will be $(\theta + 2n\pi)/\theta$ times that measured at θ . Namely, we can get a larger β_R just letting the CGW signal propagate n cycles around the circumference.

2.3. Numerical and analytical considerations

Next some numerical and analytical considerations will be conducted to understand the foregoing theoretical analyses. The given circular tube shown in Fig. 1 is assumed to be a stainless steel one with an inner radius R_1 of 104.5 mm and outer radius R_2 of 109.5 mm. The material parameters of the circular tube in Fig. 1 are given in Table 1.

Table 1. Material parameters of the circular tube.[26]

Material	Mass density $\rho/\text{kg}\cdot\text{m}^{-3}$	Longitudinal wave velocity $c_L/\text{km}\cdot\text{s}^{-1}$	Shear wave velocity $c_T/\text{km}\cdot\text{s}^{-1}$	Third-order elastic constants/GPa		
				l	m	n
Stain steel	7900	5.640	3.070	-50	-590	-720

According to the equations of stress-free boundary conditions at the inner and outer surfaces of the circular tube, the dispersion relations for CGW propagation can readily be calculated and shown in Fig. 2.[26] Considering the fact that the probes are generally located on the outer surface of the circular tube to receive the CGWs, the radius r is set to be R_2 when calculating the linear phase and group velocities.

In Fig. 2, the intersections (i.e., D_0, D_1, D_2, \dots) between the dashed line V and the DFCGW dispersion curves denote the DFCGW modes constituting the field of the second harmonic generated by the l^{th} CGW mode (point F_0 in Fig. 2) at the driving frequency $f = 0.434$ MHz. For the mode pair at $f = 0.434$ MHz (i.e., points F_0 and D_0 ; denoted by F_0 and D_0), the l^{th} primary CGW and m^{th} DFCGW strictly satisfy both

the phase and group velocity matching, and the corresponding linear phase (c_p) and group (c_g) velocities are, respectively, 4.442 km/s and 2.227 km/s. For observation of the cumulative SHG by primary CGW propagation, the specific mode pair F_0 and D_0 is selected. It should be noted that the contribution of the other DFCGWs (i.e., points D_1, D_2 , and D_3 , in Fig. 2) to the second-harmonic field of primary CGW (i.e., point F_0) can be negligible due to the mismatching of their phase velocities with $c_p^{(f,l)}$. [26] The m^{th} DFCGW mode (i.e., point D_0) plays a dominant role in $U^{(2f)}$ (see Eq. (4)).

Figure 3 illustrates the normalized displacement components of the l^{th} primary CGW mode versus the radius r . Clearly, the radial (i.e., $U_r^{(f,l)}(r) = U^{(f,l)}(r) \cdot \hat{r}$) or circumferential (i.e., $U_\theta^{(f,l)}(r) = U^{(f,l)}(r) \cdot \hat{\theta}$) component of the dis-

placement field of the l^{th} primary CGW (point F_0) is no longer exactly symmetrical or anti-symmetrical with respect to $r = (R_1 + R_2)/2$. Consequently, the field of the primary CGW mode propagating in a circular tube cannot be simply divided to be symmetric or anti-symmetric, which is quite different from Lamb waves propagating in a single isotropic plate.

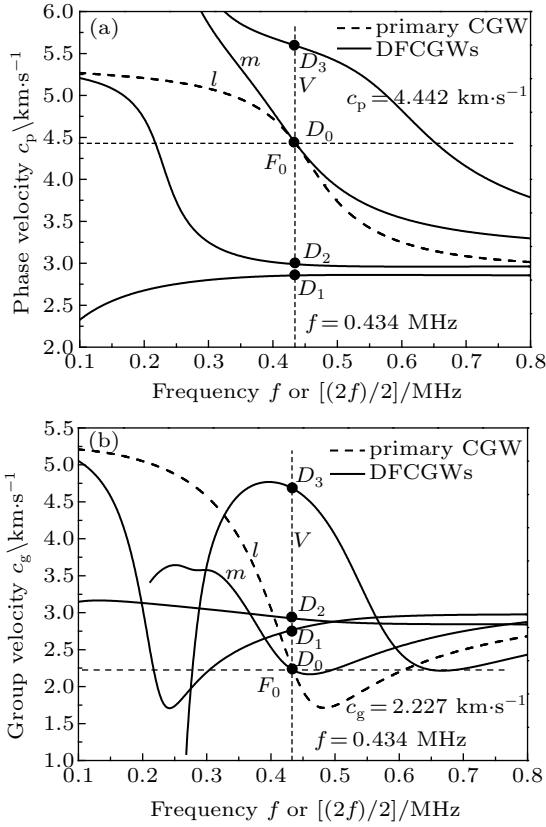


Fig. 2. Dispersion curves for the fundamental and double frequency CGWs in the given circular tube: (a) phase and (b) group velocities.

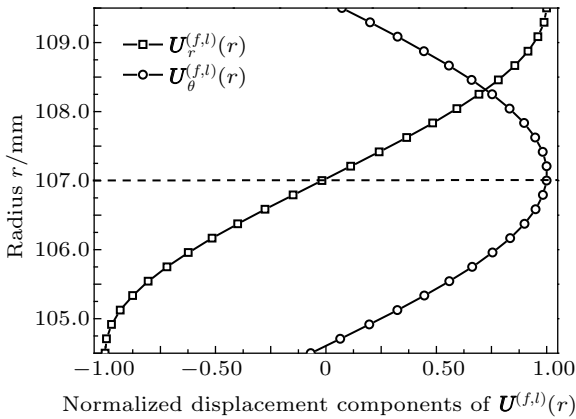


Fig. 3. Profiles of displacement components of the l^{th} primary CGW mode versus r .

It is known that the displacement field of the l^{th} CGW mode (i.e., $U_r^{(f,l)}(r)$ and $U_\theta^{(f,l)}(r)$) can be completely determined for a set of given solution $(f, c_p^{(f,l)})$ obtained from the primary CGW dispersion curve (see Fig. 2(a)). By exerting the specific displacement field ($U_r^{(f,l)}(r)$ and $U_\theta^{(f,l)}(r)$) on the circular tube, it is expected that the primary CGW mode desired

can be effectively excited. By substituting the displacement components $U_q^{(f,l)}(r)$ and $U_q^{(2f,m)}(r)$ ($q = r, \theta$) into Eqs. (4) and (5), the curve of the relative nonlinear acoustic parameter β_R at $r = R_2$ with respect to the circumferential angle θ can readily be calculated. Clearly, the relative nonlinear acoustic parameter β_R increases linearly with the circumferential angle θ because the phase velocity matching is satisfied for the mode pair F_0 and D_0 at the driving frequency $f = 0.434$ MHz (see Fig. 2). Here we use $\beta_R^{(n=1)}$ and $\beta_R^{(n=2)}$ to respectively denote the relative nonlinear acoustic parameter detected at the first and second times at the same position (e.g., point Q in Fig. 1) using the finite-duration CGW signal. Theoretically, the difference between $\beta_R^{(n=1)}$ and $\beta_R^{(n=2)}$ (denoted by $\Delta\beta_R = \beta_R^{(n=2)} - \beta_R^{(n=1)}$) at different θ ($\theta \in (0, 2\pi]$) will be the same, because $\Delta\beta_R$ represents the relative nonlinear acoustic parameter of the primary CGW propagating around one full circumference and is thus independent of θ . Clearly, based on the expression given in Eq. (5), there is $\Delta\beta_R = 2\pi |(f_m^{\text{vol}} + f_m^{\text{surf}})/(4P_{mm})| \cdot |U^{(2f,m)}(r)/[U^{(f,l)}(r)]^2|_{r=R_2}$.

3. Finite element simulations

3.1. Modeling of unidirectional CGW propagation

Generally, the CGWs generated by an excitation source exerted on the given circular tube propagate both clockwise and counterclockwise around the circumference. In the previous investigations,^[29–31] only the CGWs propagating clockwise are taken into account. To avoid the interference of CGWs that propagate counterclockwise, in the previous FE simulation model, a section cut is made on the circular tube. For investigation of enhancement effect of cumulative SHG by closed propagation feature of CGWs, it is required that the CGW signal can unidirectionally propagate (e.g., clockwise) around the full circumference. Here a model is proposed based on the coherent superposition of multi-waves to ensure the unidirectional propagation of primary CGW around the full circumference. As shown in Fig. 1, the angle $\Theta = \widehat{AB}/R_2$ between two exactly the same (coherent) excitation sources S_1 and S_2 is set to be $\lambda/(4R_2)$ (i.e., the arc length \widehat{AB} is $\lambda/4$), where λ is the wavelength of the l^{th} primary CGW mode desired, and the phase of the source S_1 is set to be $\pi/2$ ahead of that of S_2 . Assuming that the amplitudes of both waves generated respectively by S_1 and S_2 are A , and that they remains constant during the propagation process. The points P and Q are, respectively, two arbitrary probe points in the counterclockwise and clockwise directions (see Fig. 1). At the arbitrary point P , the phase difference $\Delta\phi$ between the two CGWs, generated respectively by S_1 and S_2 and propagating counterclockwise, is given by

$$\Delta\phi = \phi_2 - \phi_1 - (2\pi/\lambda) \cdot \widehat{\Delta}, \quad (6)$$

where $\widehat{\Delta} = \widehat{PA} - \widehat{PB} = \widehat{AB}$, ϕ_i ($i = 1, 2$) is the phase of the source S_i , and $\phi_2 - \phi_1 = -\pi/2$. For the arbitrary probe point P in Fig. 1, the phase difference $\Delta\phi$ is readily found to be $-\pi$. That is, when the two CGWs are respectively generated by S_1 and S_2 and propagate counterclockwise around the circumference, the phase difference between them is always π at the arbitrary point P . Theoretically, the amplitude of wave detected at the arbitrary probe point P is equal to zero. It can be deduced that there is no desired CGW propagating counterclockwise around the circumference. In the same way, for the arbitrary probe point Q , there are $\widehat{\Delta} = \widehat{QA} - \widehat{QB} = -\lambda/4$ and $\Delta\phi = 0$ in Eq. (6). That is, when the two CGWs are respectively generated by S_1 and S_2 and propagate clockwise around the circumference, the phase difference between them is always zero at the arbitrary point Q . Thus the amplitude of wave detected at the arbitrary point Q is equal to $2A$. Based on the model presented here, it is expected that the unidirectional propagation of the primary CGW around the full circumference will take place.

3.2. Finite element simulations on enhancement effect

Here, FE simulations on enhancement effect of the cumulative SHG by closed propagation feature of CGWs are conducted using a commercial software COMSOL 5.3[®]. The model used for FE simulations is also shown in Fig. 1, where the geometrical and materials parameters of the circular tube are the same as that given in Subsection 2.3. The Murnaghan model and plane strain conditions are used.^[34] To guarantee the high efficiency and error convergence, the mapped element type of 0.25 mm is used to discretize the model. To satisfy the stability analysis, the time step Δt is chosen to be 0.02 μs in FE simulations. Two exactly the same excitation sources S_1 and S_2 with the specific displacement field distribution of the primary CGW mode (i.e., point F_0 in Fig. 2) are applied in the given circular tube to generate the unidirectional CGW propagation (see Fig. 1). To effectively generate the pure primary CGW mode desired and to inhibit unwanted CGW modes, the prescribed displacement distributions applied on two exactly the same excitation sources S_1 and S_2 are set to be $D_q(r, t) = T_0 A_q(t) U_\theta^{(f, l)}(r)$ ($q = 1, 2$), where T_0 is the amplitude, and its value is set to be 1 μm ; $U_\theta^{(f, l)}(r)$ is the field function of circumferential displacement component of the primary CGW mode (point F_0 in Fig. 2), as that shown in Fig. 3; $A_q(t)$ ($q = 1$ and 2) are the tone-burst temporal waveform consisting of N cycles of Hanning windowed sine signal, which are, respectively, defined as $A_1(t) = \sin(2\pi f_0 t + \pi/2) \times [1 - \cos(2\pi f_0 t/N)]$ and $A_2(t) = \sin(2\pi f_0 t) \times [1 - \cos(2\pi f_0 t/N)]$.^[35] In FE simulations, the central frequency f_0 and the cycle number N are, respectively, set to be 0.434 MHz and 49. Stress free boundary conditions are applied on the inner and outer surfaces of

the circular tube, and the probe points (see Fig. 1) are positioned on the outer surface to pick up the radial displacement component.

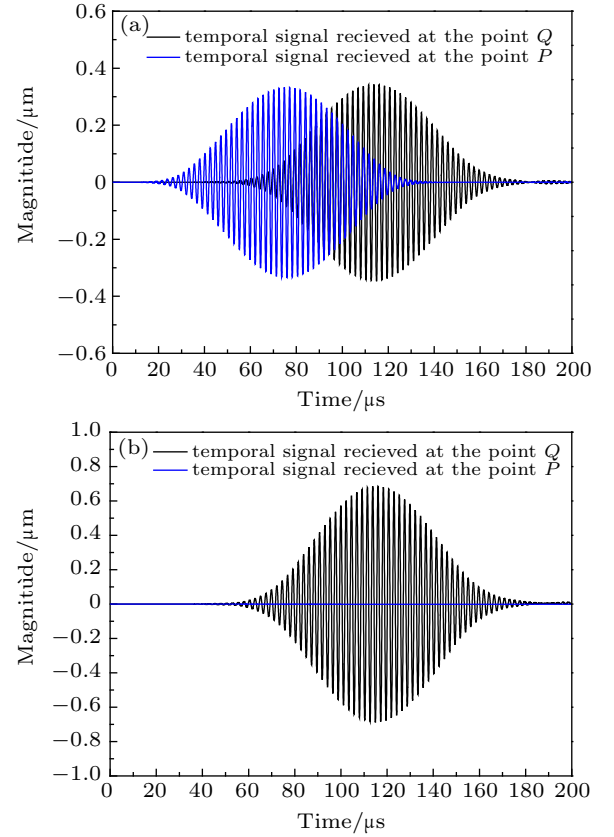


Fig. 4. Temporal signals received at points P and Q in Fig. 1; (a) only S_1 is driven by $D_1(r, t)$, and (b) both S_1 and S_2 are simultaneously driven by $D_1(r, t)$ and $D_2(r, t)$.

In the model shown in Fig. 1, the enhancement effect of SHG by the closed propagation feature of unidirectional CGW propagation in the given circular tube is modeled and simulated with FE simulations. First of all, it is necessary to verify that the model of FE simulations can effectively excite the desired unidirectional CGW signal. When only the excitation source S_1 is driven by the prescribed displacement $D_1(r, t)$, the temporal signals respectively received at the probe points P and Q in Fig. 1 are shown in Fig. 4(a). Obviously, both the temporal signals are remarkable, which means that the CGW signals propagating clockwise and counterclockwise along the circumference are generated simultaneously. When the two exactly same excitation sources S_1 and S_2 are simultaneously driven by the prescribed displacements $D_1(r, t)$ and $D_2(r, t)$, the temporal signals respectively received at the probe points P and Q are shown in Fig. 4(b). Clearly, the temporal signal received at the probe point P almost disappears completely while the temporal signal received at the probe point Q almost increases two times than that in Fig. 4(a). This FE simulation result is completely consistent with the prediction based on modeling of unidirectional CGW propagation given in Subsection 3.1. Considering the similar physical features of guided

wave propagation, it is expected that the modeling of unidirectional CGW propagation presented here is also suitable for other guided waves such as Lamb waves propagating in plate-like structures.

Next, the enhancement effect of SHG by the closed propagation feature of unidirectional CGW propagation will be examined by FE simulations, which has been analyzed in Subsection 2.2. When the primary CGW signal [like that in Fig. 4(b)] propagates clockwise in the circular tube, the first two clear time-domain signals [denoted by C and D in Fig. 5(a)] can be detected at the probe point positioned at an appropriate circumferential angle (e.g., $\theta = \pi/2$) as long as the time frame is set to be long enough, which is consistent with the results measured in our previous experimental work.^[28] Theoretically, the group delay of the primary CGW mode desired [i.e., point F_0 in Fig. 2(a); $c_g^{(f)} = 2.227$ km/s] around one full circumference of the tube examined is calculated to be $2\pi R_2/c_g^{(f)} = 308.93$ μs , which is very close to the group delay $\Delta t = 310.12$ μs between the two signals C and D (R.E. 0.395%). Hereby, the carrier of the signals C and D is certainly the CGW mode (point F_0), and their corresponding propagation circumferential angles are, respectively, $\pi/2$ and $2\pi + \pi/2$ in Fig. 1. The spectrogram obtained by using short time Fourier transform (STFT) for the time-domain signal shown in Fig. 5(a) is illustrated in Fig. 5(b), where the frequencies of the fundamental wave and second harmonic

generated are marked with the dotted horizontal lines (H_1 and H_2). The two slices along the dotted horizontal lines H_1 and H_2 are, respectively, shown in Figs. 5(c) and 5(d), through which the corresponding amplitudes of the primary CGW at $f = 0.434$ MHz (point F_0) and the second harmonic generated at $f = 0.868$ MHz, denoted by $A_1^{(q)}$ and $A_2^{(q)}$ (where $q = C$ or D corresponds to the signal C or D), can readily be determined. Also, it can be observed that the signal magnitude of primary CGW remains almost constant, while the signal magnitude of the second harmonic generated at $\theta = \pi/2$ is obviously smaller than that at $\theta = 2\pi + \pi/2$, which is consistent with the theoretical prediction where the second harmonic generated grows along the tube circumference. By analyzing the time-domain signals shown in Fig. 5(a) and the STFT results shown in Figs. 5(b), 5(c) and 5(d). It is convinced that the CGW mode desired can be selectively excited using the FE simulation model established in Fig. 1. Based on the amplitudes of primary CGW and second harmonic generated [i.e., $A_1^{(q)}$ and $A_2^{(q)}$ in Figs. 5(c) and 5(d)], the corresponding $\beta_R^{(n=1)} = A_2^{(C)}/[A_1^{(C)}]^2$ and $\beta_R^{(n=2)} = A_2^{(D)}/[A_1^{(D)}]^2$, as well as $\Delta\beta_R = \beta_R^{(n=2)} - \beta_R^{(n=1)}$ can readily be determined, where $\beta_R^{(n=1)}$ and $\beta_R^{(n=2)}$ are, respectively, the relative nonlinear acoustic parameter detected at the first and second times at the same position ($\theta = \pi/2$) using the finite-duration CGW signal (see Subsection 2.3).

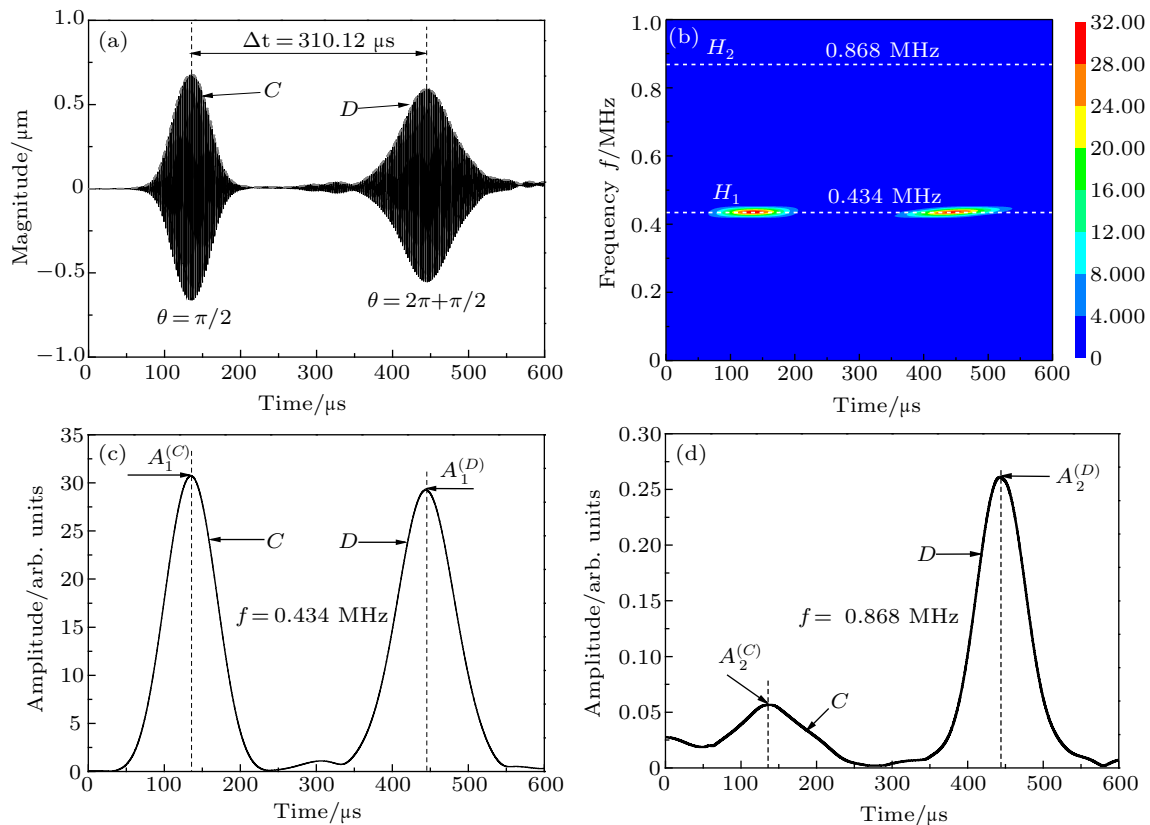


Fig. 5. (a) Time-domain signal detected at the probe point $\theta = \pi/2$, (b) the corresponding spectrogram, (c) the slice at the fundamental frequency (line H_1), and (d) the slice at the second-harmonic frequency (line H_2).

The probe points are placed around the outer surface of the given circular tube (see Fig. 1), where the propagation circumferential angle θ is set to be changed from $\pi/8$ rad to $15\pi/16$ with an interval of $\pi/8$. For different probe points, the time-domain signal similar to that shown in Fig. 5(a) can be simulated, then the values of $A_1^{(q)}$ and $A_2^{(q)}$ like that shown in Figs. 5(c) and 5(d) can be calculated by using STFT. The corresponding values of $\beta_R^{(n=1)}$ and $\beta_R^{(n=2)}$, as well as $\Delta\beta_R$, can readily be determined subsequently, and these parameters with respect to the propagation circumferential angle θ are shown in Fig. 6. Obviously, the results of FE simulations are reasonably consistent with the theoretical predictions. Figure 6(a) illustrates that the amplitude of the second harmonic generated will linearly increase with propagation circumferential angle θ in each propagation cycle when the strict phase velocity matching and nonzero power flux are simultaneously satisfied (see mode pair F_0 and D_0 in Fig. 2). It can be found in Fig. 6(b) that the parameter $\Delta\beta_R$ measured at different θ is almost kept the same. Obviously, the FE simulations performed are completely consistent with the theoretical and analytical considerations involving the enhancement effect of cumulative SHG by closed propagation feature of CGW in Section 2.

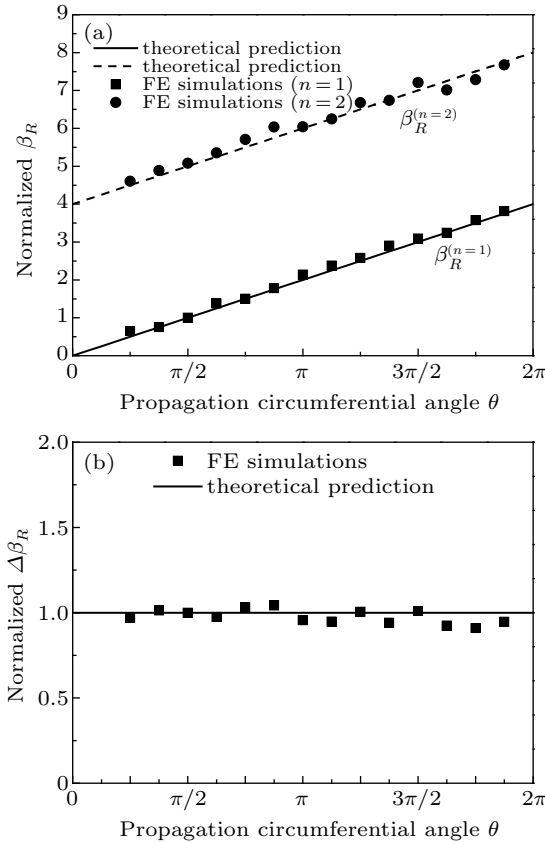


Fig. 6. Normalized relative nonlinearity parameter of primary CGW versus θ : (a) $\beta_R^{(n=1)}$ and $\beta_R^{(n=2)}$, and (b) $\Delta\beta_R$.

4. Discussion

The results of aforementioned theoretical considerations and FE simulations have verified that the closed propagation feature of CGWs can enhance the effect of cumulative second

harmonic generated. What we are more interested in is how to apply this closed propagation feature of CGWs in practical applications. Generally, the potential is mainly reflected from the following aspects.

Firstly, the source of nonlinearity can be effectively distinguished using the enhancement effect of cumulative SHG by closed propagation feature of CGWs. It is known that in the measurement of second harmonics generated by primary guided wave propagation, the nonlinearity of the measurement system composed of signal generator, power amplifier, ultrasonic transducer, couplant and so on will lead to the appearance of an extra second-harmonic signal. This extra second-harmonic signal may be even larger than that induced by defects in material. Generally, it is difficult to distinguish the measured second-harmonic signal whether from the measurement system, material itself or both. It is worth noting that the material nonlinearity of interest can be distinguished from the measurement system using the enhancement effect of cumulative SHG by closed propagation feature of CGWs. Take our previous experimental investigation as an example,^[28] when the wedge transmitting transducer for generation of the desired primary CGW is driven by the specified tone-burst voltage, the receiving wedge transducer successively receives two clear time-domain signals similar to that in Fig. 5(a), and the corresponding $\beta_R^{(n=1)}$ and $\beta_R^{(n=2)}$, as well as $\Delta\beta = \beta_R^{(n=2)} - \beta_R^{(n=1)}$ can readily be determined. Generally, the origin of $\beta_R^{(n=1)}$ includes two aspects: the nonlinearity of the measurement system (including couplant) and the material nonlinearity of the circular tube through which the primary CGW propagates along the path of θR_2 ,^[28] while the origin of $\beta_R^{(n=2)}$ is the same as that of $\beta_R^{(n=1)}$ except for the difference in the length of propagation path (i.e., $\theta R_2 + 2\pi R_2$). Thus, the relative acoustic nonlinearity parameter $\Delta\beta = \beta_R^{(n=2)} - \beta_R^{(n=1)}$ completely eliminates the influence of the measurement system (including couplant), and quantitatively characterizes the material nonlinearity of the circular tube through which the primary CGW propagates through one full circumference.^[28]

Secondly, the detection sensitivity of early damage stage can be improved using the enhancement effect of cumulative SHG by closed propagation feature of CGW. Previous investigations indicate that in the early damage stage of material, change in the second-order elastic constants (SOECs) of material is inconsiderable, and variation in the relative nonlinear acoustic parameter should be mainly attributed to change in the three-order elastic constants (TOECs) of material.^[21] To facilitate the investigation of assessing early damage in material (characterized by change in TOECs) by using the relative nonlinear acoustic parameter, the TOECs are assumed to change from its initial values (A, B, C) to $r_c \times (A, B, C)$,^[31] where r_c is the damage status coefficient used to describe the degree of early damage, while the remaining material properties and geometric parameters of the circular tube are kept unchanged. Base on Eq. (5), the curves of normalized $\beta_R^{(n=1)}$, $\Delta\beta_R = \beta_R^{(n=2)} - \beta_R^{(n=1)}$ and $\Delta\beta'_R = \beta_R^{(n=3)} - \beta_R^{(n=1)}$ detected at

an appropriate circumferential angle (e.g., $\theta = \pi/4$) versus the scale coefficient r_c are shown in Fig. 7, where r_c varies from 1.0 to 1.5 with an interval of 0.1. Obviously, $\Delta\beta_R$ and $\Delta\beta'_R$ are more sensitive to early damage of the tube material than $\beta_R^{(n=1)}$. It can also be seen that the detection sensitivity to the early damage is further improved by properly increasing propagation cycle number n , that is, $\Delta\beta'_R$ is more sensitive to early damage than $\Delta\beta_R$.

Theoretically, increasing the propagation cycle number n can improve the detection sensitivity to the early damage. However, it should be noted that increasing the propagation cycle number n is equivalent to increasing the propagation path. Practically, the propagation attenuation of CGWs will inevitably increase with the propagation cycle number n , which will reduce the signal-to-noise ratio (SNR). Thus, it is necessary to find a balance between keeping an appropriate SNR and improving the detection sensitivity of early damage in practical measurements.

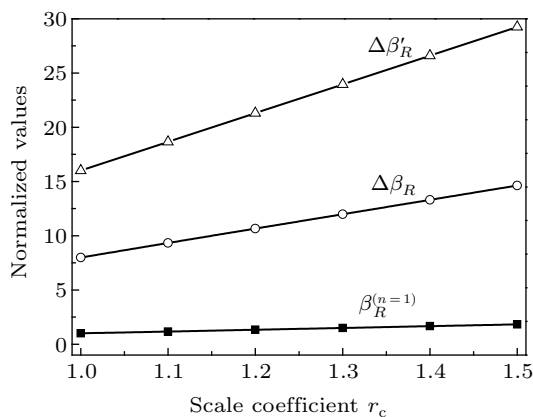


Fig. 7. Curves of normalized $\beta_R^{(n=1)}$, $\Delta\beta_R$ and $\Delta\beta'_R$ versus the scale coefficient of TOECs.

5. Conclusions

A theoretical model is established for analyzing the enhancement effect of cumulative SHG by the closed propagation feature of CGWs in a circular tube. Using a second-order perturbation and a modal expansion analysis, the mathematical expression of the second-harmonic fields by primary CGW propagation in a circular tube has been derived. In order to realize the unidirectional propagation of CGWs, a model is proposed based on coherent superposition of multi-waves to ensure the unidirectional propagation of primary CGWs around the full circumference. Regarding the enhancement effect of cumulative SHG by the closed propagation feature of CGWs, some numerical and analytical considerations are performed, and then FE simulations are conducted to further validate the said effect. A close agreement between the theoretical predictions and FE simulations verifies the effectiveness of using the model based on the coherent superposition of multi-waves to realize the unidirectional propagation of primary CGWs, and the enhancement effect of cumulative SHG by closed propagation feature of CGWs. On this basis, the potential for applications of the closed propagation feature of CGWs are considered and discussed. It is convinced that, in the SHG

based nonlinear measurements, the enhancement effect of cumulative SHG by closed propagation feature of CGWs can be used to effectively remove the unwanted nonlinearity coming from the measurement system. In addition, with the enhancement effect of cumulative SHG by closed propagation feature of CGWs, the detection sensitivity of early damage of circular tube can be improved, especially when the SHG effect of CGW propagation is not enough to accurately characterize the early damage of material. The potential mentioned here is expected to play an important role in the nonlinear CGW detection technology. The results obtained here yield a previously unavailable insight into the physical mechanism of the enhancement effect of cumulative SHG by closed propagation feature of CGWs in a circular tube.

References

- [1] Wang H, Han J and Hui Z 2013 *Applied Mechanics and Materials* **278** 487
- [2] Zeng D, Deng K, Shi T and Lin Y 2014 *J. Press. Vessel Tech.* **136** 061402
- [3] Ditre J J 1994 *J. Acoust. Soc. Am.* **96** 3769
- [4] Li J and Rose J L 2001 *J. Acoust. Soc. Am.* **109** 457
- [5] Hayashi T and Murase M 2005 *J. Acoust. Soc. Am.* **117** 2134
- [6] Wang X J, Tse P W, Mechefske C K and Hu M 2010 *NDT&E Int.* **43** 365
- [7] Barshinger J N and Rose J L 2004 *IEEE Trans. Ultrasonics, Ferroelectrics, and Frequency Control* **51** 1547
- [8] Demma A, Cawley P, Lowe M and Roosenbrand A G 2003 *J. Acoust. Soc. Am.* **114** 611
- [9] Li J and Rose J L 2001 *J. Acoust. Soc. Am.* **109** 457
- [10] Liu G and Qu J 1998 *J. Appl. Mech.* **65** 424
- [11] Valle C, Qu J and Jacobs L J 1999 *Int. J. Eng. Sci.* **37** 1369
- [12] Qu J, Berthelot Y and Li Z 1996 *Review of Progress in Quantitative Nondestructive Evaluation* **15** 169
- [13] Valle C, Niethammer M, Qu J and Jacobs L J 2001 *J. Acoust. Soc. Am.* **110** 1282
- [14] Yu J and Wu B 2009 *Eur. J. Mech. A-Solid* **28** 560
- [15] Yeh C H and Yang C H 2011 *Ultrasonics* **51** 472
- [16] Gao G J, Deng M X, Li M L and Liu C 2015 *Acta Phys. Sin.* **64** 224301 (in Chinese)
- [17] Deng M X and Pei J F 2007 *Appl. Phys. Lett.* **90** 121902
- [18] Xiang Y X and Deng M X 2008 *Chin. Phys. B* **17** 4232
- [19] Liu Y, Khajeh E, Lissenden C J and Rose J L 2013 *J. Acoust. Soc. Am.* **133** 2541
- [20] An Z W, Wang X M, Li M X, Deng M X and Mao J 2009 *Chin. Phys. Lett.* **26** 114302
- [21] Nagy P B 1998 *Ultrasonics* **36** 375
- [22] Deng M X and Xiang Y X 2010 *Chin. Phys. B* **19** 114302
- [23] Jhang K Y and Kim K C 1999 *Ultrasonics* **37** 39
- [24] Kim C S and Jhang K Y 2012 *Chin. Phys. Lett.* **29** 060702
- [25] Xiang Y X, Zhu W J, Deng M X and Xuan F Z 2016 *Chin. Phys. B* **25** 024303
- [26] Gao G J, Deng M X and Li M L 2015 *Acta. Phys. Sin.* **64** 184303 (in Chinese)
- [27] Deng M X, Gao G J and Li M L 2015 *Chin. Phys. Lett.* **32** 124305
- [28] Deng M X, Gao G J, Xiang Y X and Li M L 2017 *Ultrasonics* **75** 209
- [29] Li M L, Deng M X and Gao G J 2016 *Acta Phys. Sin.* **65** 194301 (in Chinese)
- [30] Li M L, Deng M X, Gao G J and Xiang Y X 2018 *J. Sound Vib.* **421** 234
- [31] Li M L, Deng M X, Gao G J and Xiang Y X 2018 *Ultrasonics* **82** 171
- [32] Li M L, Liu L B, Gao G J, Deng M X, Hu N, Xiang Y X and Zhu W J 2019 *Chin. Phys. B* **28** 044301
- [33] Deng M X 2003 *J. Appl. Phys.* **94** 4152
- [34] Chillara V and Lissenden C 2014 *Ultrasonics* **54** 1553
- [35] Wan X, Tse P, Xu G and Tao T 2016 *Smart Mater. Struct.* **25** 045023